

Article

Application of Tesla Valve's Obstruction Characteristics to Reverse Fluid in Fish Migration

Guorui Zeng¹ , Maosen Xu^{1,2,*} , Jiegang Mou^{1,2}, Chenchen Hua¹ and Chuanhao Fan¹¹ College of Metrology and Measurement Engineering, China Jiliang University, Hangzhou 310018, China² Zhejiang Engineering Research Center of Smart Fluid Equipment & Measurement and Control Technology, Hangzhou 310018, China

* Correspondence: msxu@cjlu.edu.cn

Abstract: More and more activities have caused significant damage to the river environment, among which a typical problem of blocked fish migration is constantly attracting people's attention. Nowadays, fishways are essential hydraulic facilities to solve such problems. Although a different fishway has a particular blocking effect on the water flow, the flow velocity of the vital positions of fish migration in the fishway could still be relatively high locally, which may pose a certain challenge to the fish migration (the higher flow velocity could lead to the increase in migratory energy consumption of fish). Therefore, further exploration of fish passing facilities may be required. As a check valve without movable parts, the Tesla valve is expected to be used in fish passing facilities because of its substantial obstruction to the reverse flow of internal fluid. This paper conducted numerical simulation experiments on the fish passage pipeline designed based on Tesla valves using the RNG (renormalization group) $k-\epsilon$ model. Grass carp were selected as the primary analysis object, and the simulation results were analyzed from the perspective of turbulence characteristics. The results showed that the fish passage pipeline based on the T45-R Tesla valve was better than that on the GMF (Gamboa, Morris and Forster) Tesla valve in velocity control. The velocity at the vital position of T45-R internal fluid was about 20% lower than that of GMF. The results of the velocity cloud diagram showed apparent high-velocity and low-velocity areas in the fish passage pipeline designed based on the T45-R Tesla valve. The high-velocity area was the vital position for fish upstream, and the maximum velocity variation range in this area was 0.904~1.478 m/s. At the same time, the flow in the low-velocity area is almost static water. The analysis illustrated that the resulting velocity environment could provide conditions for grass carp to move upstream successfully. The results of turbulent kinetic energy inside the fish passage pipeline showed that the maximum value of turbulent kinetic energy was only about $0.043 \text{ m}^2/\text{s}^2$, which could be friendly for fish upstream. In addition, the results show that pressure-related problems could not seem to have an excessive impact on fish migration, such as causing damage. Overall, the results further studied the feasibility of using the Tesla valve as a fish passage pipeline.



Citation: Zeng, G.; Xu, M.; Mou, J.; Hua, C.; Fan, C. Application of Tesla Valve's Obstruction Characteristics to Reverse Fluid in Fish Migration. *Water* **2023**, *15*, 40. <https://doi.org/10.3390/w15010040>

Academic Editor: Xiaoming Jiang

Received: 14 November 2022

Revised: 19 December 2022

Accepted: 19 December 2022

Published: 22 December 2022

Keywords: fish migration; Tesla valve; turbulence characteristics; grass carp

Copyright: © 2022 by the authors. Licensee MDPI, Basel, Switzerland. This article is an open access article distributed under the terms and conditions of the Creative Commons Attribution (CC BY) license (<https://creativecommons.org/licenses/by/4.0/>).

1. Introduction

Fish migration refers to fish's periodic directional back-and-forth movement due to physiological requirements, and genetic and environmental factors. Respecting the rules of fish migration is integral to restoring the natural ecology. However, current human activities, such as hydropower generation or other water abstraction for industry make wild fish face the hassle of migration obstruction [1–3]. The obstruction of fish migration will cause significant damage to the habits of fish, such as feeding, reproduction, and avoiding predation [4,5]. It may cause a significant reduction in the fish population size, further deterioration, and may cause serious consequences, such as interruption of gene exchange and even species extinction [6]. Nowadays, different fish passing facilities are

often used to solve the problem of blocked fish migration, and the fishway is widely used [7]. Currently, the fishway is mainly divided into traditional types (i.e., vertical slot, orifice, and overflow weir fishway) and multiple fishway combination types. Although the traditional fishway has a certain energy dissipation effect on the water flow, the flow velocity of the vital positions of fish migration in the fishway could still be relatively high locally [8,9]. The combined fishway integrates some hydraulic characteristics of different fishways but still has problems, such as complex structure and complicated design [10]. At the same time, although fish locks and fish elevators occupy a small area, these fish passing facilities may have problems, such as difficulty in attracting fish and high costs for long-term operation [11]. Therefore, it is necessary to design a fish passing facility with high efficiency, simple structure, and low cost to solve the problem of hindered fish migration, considering the development direction of ecological restoration in the future and the existing issues in the current fish passing facilities.

A Tesla valve is a check valve proposed by Nikola Tesla in 1920. It is characterized by allowing the fluid to flow easily in one direction, but the fluid suffers strong resistance in the opposite direction. In addition, the Tesla valve without movable parts has the advantages of a simple structure, long service life, and convenient processing [12]. Due to its excellent performance, the Tesla valve may have the potential to be used in a fishway. In 2016, Delft University of Technology (Netherlands) [13] proposed the possibility of a large-scale Tesla valve applied to the fishway and conducted hydraulic model experiments. It was found that the Tesla valve has a specific potential to be applied to fishway construction. Their series of experiments judged from the perspective of general experience (i.e., a pond–stream–pond structure that allows fish to migrate in a series of small steps [14]) and found that the unit's flow rate and flow pattern composed of a Tesla valve could meet the requirements after the fluid passes through under specific working conditions. Different researchers also present relevant results in the research of Tesla valve pipelines. Clear high- and low-speed regions and strong water-blocking capacity are likely to provide conditions for fish migration [15,16]. However, due to the limitation of experimental conditions, the critical data were lacking and not enough to evaluate the performance of the Tesla valve as fishways. Moreover, further development of the study may involve the adjustment of the model [17]. Therefore, further research is needed.

The methods to study fishways can be classified into hydraulic model experiment, numerical simulation, and passing fish experiment. Tarrade, et al. [18] constructed a typical full-size vertical slot fishway hydraulic model and studied various flow parameters and flow evolution stages in the model in the experiment. Dong, et al. [19] also studied the turbulence structure of the combined fishway through a hydraulic test. They measured the three-dimensional instantaneous velocity in the fishway using acoustic Doppler velocimetry (ADV) and analyzed the turbulence characteristics in the fishway pool using jet mechanics and turbulence statistics theory. However, the experimental method of the hydraulic model has the problem of a single research object, and more models usually mean more experimental cost investment. Duarte, et al. [20] added the fish passage experiment based on the fishway hydraulic model. Although the biological test can reflect the effect of fish passage to a certain extent, a simultaneous in-depth hydraulic characterization is needed. The results from biological tests are easily affected by many factors, which may introduce uncertainty to the conclusions. Among many research methods, numerical simulation is an effective method for the early feasibility verification of research objectives [21,22]. For example, Heimerl, et al. [23] used a numerical simulation method to simulate the three-dimensional flow of fishway by CFX (Computational Fluid Dynamics Software, no version number given by the original source, ANSYS, Pittsburgh, Pennsylvania, USA) and conducted a refined study of the flow velocity distribution. Fuentes-Perez, et al. [24] carried out numerical simulation experiments based on Open FOAM (Open FOAM 3.0.1, CFD Direct, Reading, UK), and standard $k-\varepsilon$ and large eddy simulation (LES) Smagorinsky models were selected, which proved the necessity of a 3D model to describe nonuniformity correctly.

Similarly, Marriner, et al. [25] conducted a comprehensive assessment of the hydraulics of Canada's Vianney Legendre vertical slot with the help of numerical tools. The fishway has been proven to pass various fish species successfully. In addition, Barton and Keller [26] carried out numerical simulation experiments, used the RNG $k-\epsilon$ model (based on the renormalization group theory) to simulate the 3D vertical slot fishway with a free surface, and obtained the detailed velocity field information of different water depths of the vertical slot; satisfactory results were obtained. These results also provide essential guidance for the later experimental design. At the same time, the microstructure of flow, such as turbulence, has an important impact on the success of fish upstream. Silva et al. [27] studied the effects of velocity, turbulent kinetic energy, and Reynolds shear stress on fish abduction behavior in the fishway of the pond chamber through a fish passing test. The turbulence characteristics of fish passage facilities are critical indicators to judge whether fish can migrate successfully. However, the fine turbulent structure is difficult to be measured by experimental method. Therefore, numerical simulation is an important research method for the turbulent characteristics of fishways [28,29].

For an ideal fish passage, a structure is required to have a continuously open connection between both sides of the migration barrier, while preventing high flow around the barrier [13]. The Tesla valve has strong obstruction characteristics for reverse flow and has the advantages of a simple structure and no movable parts. Therefore, the Tesla valve could have the possibility of being used as an ideal fishway. The innovation of this study was to discuss the possibility of Tesla valve being used as a passing fish facility in the form of a pipeline. Specifically, this study numerically simulated the turbulence characteristics, energy dissipation, and pressure-related problems of the fish passage pipeline designed by the T45-R Tesla valve and GMF Tesla valve, respectively, which may enrich the lack of relevant research on the application of Tesla valves in fish migration scenarios. The swimming ability data of different fishes were also analyzed as the fish passage target to evaluate the feasibility of applying the fish passage pipeline in the early stage. This study may help provide a reference for new research ideas on the fishway.

2. Materials and Methods

2.1. Physical Model

T45-R is one of the standard models among Tesla valves, with broad application prospects [30]; GMF Tesla valve is a typical representative of good performance [31]. Therefore, these two Tesla valves were selected as the research objects. The size structure of the two Tesla valves is shown in Figure 1, and all feature information is indicated. According to K. Keizer's experiment [13], this numerical simulation adopted six basic units of two types of Tesla valves to form two kinds of passing fish pipelines, as shown in Figure 2 (the vital locations of migration have been marked in the figure). The length of the inlet and outlet of the fish passage pipe model was appropriately extended to reduce the impact of the inlet and outlet on the simulation experiment. In order to simplify the preliminary experiment, the model size was numerically simulated according to the size given in Figure 1 to determine a more suitable fish passage pipe for the following numerical calculation.

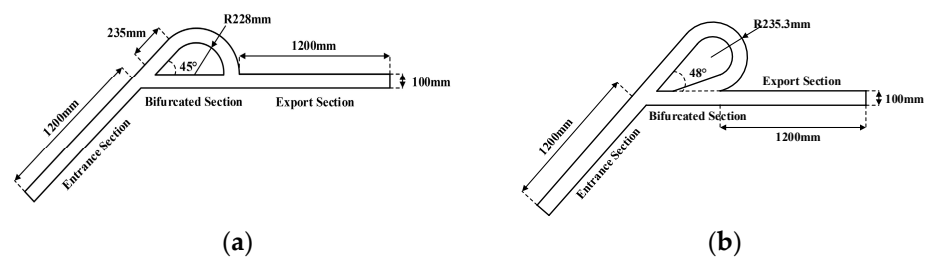


Figure 1. Schematic diagram of size and structure of two Tesla valves (mm) ((a) T45-R, (b) GMF, and the width of entrance is 100 mm).

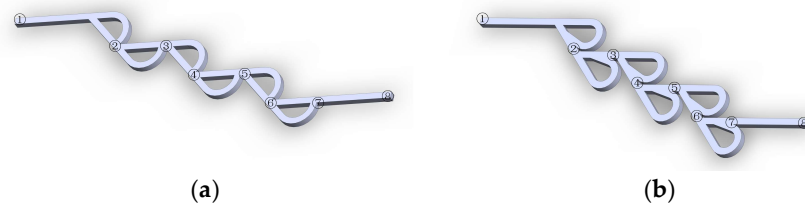


Figure 2. Schematic diagram of two fish passing pipeline models based on Tesla valve ((a) fish passing pipe designed based on T45-R, (b) fish passing pipe designed based on GMF; the vital positions for testing have been marked with numbers in the figure).

2.2. Numerical Calculation

After establishing the model in the previous section, the mesh of the above two physical models was divided, and the mesh type was the structured grid. The part of the model that needed a satisfactory solution was encrypted after verifying mesh independence, a numerical simulation experiment based on Fluent 19.1 (ANSYS, Pittsburgh, Pennsylvania, USA.). The total number of the mesh of all models was controlled at about 950,000 (as the independence verification of the grid relies on the results of reliability verification of numerical methods, the relevant contents are arranged in Section 2.3), and the mesh quality was higher than 0.9. An example of the grid model is shown in Figure 3.

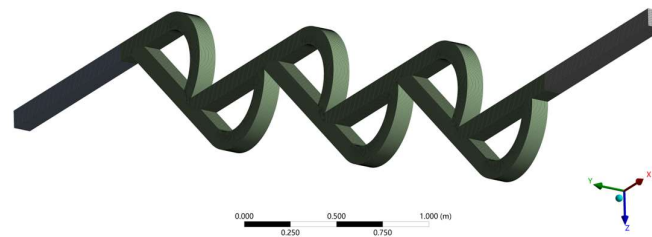


Figure 3. Schematic diagram of meshing (T45-R).

RNG $k-\varepsilon$ turbulence model was adopted in this paper because the model object used in this numerical simulation was a special type of stop valve, which was verified by numerical simulation and experimental results [32]. The researchers found that the RNG $k-\varepsilon$ model had a good simulation for the 3D turbulence of the stop valve, and the results were in good agreement with the actual values. In addition, the comparison of multiple models commonly used in the three-dimensional numerical simulation of fishways has been studied. It found that the RNG $k-\varepsilon$ model can reflect the flow structure of fishway well and save computing resources relatively [33]. Therefore, the RNG $k-\varepsilon$ model used here may be suitable for this scenario, where the valve is combined with the fishway.

As shown in Figure 4, in the numerical calculation, gravity was decomposed into F_x and F_y to simulate the situation of the fish pipeline under different slopes θ (the slope of the initial comparison test was 0%, 5%, and 10%, respectively). The boundary condition was set as the velocity inlet (the velocity of the initial comparison test was 0.3 m/s, 0.6 m/s, and 0.9 m/s, respectively). The SIMPLE pressure–velocity coupling algorithm was adopted. The second-order upwind style discretization was adopted. Standard wall parameters were selected for each wall. The number of iteration steps was set at 2000 and the convergence accuracy was 10^{-3} .

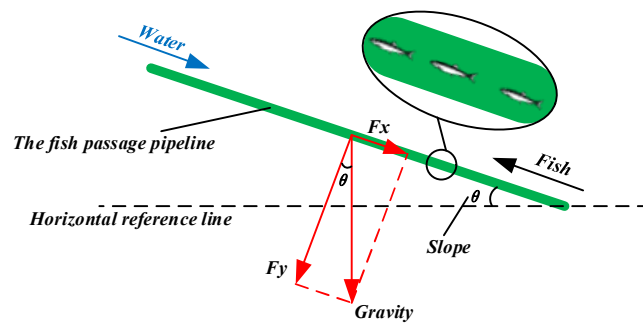


Figure 4. Gravity decomposition diagram of fish passage pipeline.

2.3. Numerical Calculation Verification

In order to verify the reliability of the numerical calculation method, the numerical method was applied to the simulation of a six-stage T45-C Tesla valve with the same series and high similarity to the research object. The results were compared with the research results of Bao and Wang [34]. The model specifications and all numerical setting schemes were consistent with those mentioned in the previous section. The relative pressure drop ratio (RPDR) and absolute pressure drop ratio (APDR) can comprehensively and effectively evaluate the performance of the Tesla valve. They were selected as two parameters to verify the accuracy of the numerical calculation method in this paper (the calculation formulas of RPDR and APDR are shown in Formulas (1) and (2)). The model mesh was divided into four schemes, with the number of mesh being about 740,000, 950,000, 1,200,000, and 1,310,000, respectively. As shown in Figure 5, when the number of mesh exceeded 950,000, the error caused by the number of mesh was small. Considering the calculation resources and accuracy, the number of structural grids was about 950,000.

$$RPDR = (\Delta P_r - \Delta P_e) / (\Delta P_f - \Delta P_e) \tag{1}$$

$$APDR = (\Delta P_r - \Delta P_f) / \Delta P_e \tag{2}$$

where ΔP_f is the pressure drop in forward flow, ΔP_r is the pressure drop in reverse flow, and ΔP_e is the pressure drop of the corresponding pure pipeline.

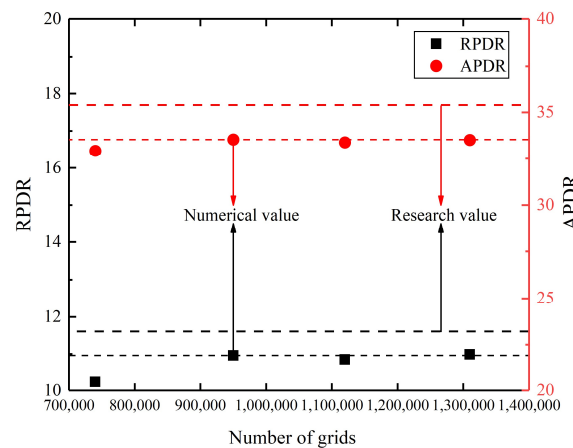


Figure 5. The verification of mesh independence.

When the number of mesh was about 950,000, the numerical detail results are shown in Table 1. The numerical results given by this method were close to the corresponding research results, and the error was acceptable in engineering applications. At the same time, because the experimental object was similar to the structure of the T45-C Tesla valve, it showed that the numerical method used in this paper was credible [35,36].

Table 1. Comparison of research results.

	Research Results	Numerical Results	Relative Error (%)
RPDR	11.61	10.96	5.60%
APDR	35.83	33.54	6.39%

2.4. Target Fish

The main fish passing analysis object selected in this paper was grass carp (*Ctenopharyngodon idella*), a semi-migratory fish and one of the common fish in nature [37,38]. It is naturally mainly distributed in China, Russia, and Bulgaria. It is mainly distributed in the Yangtze River, the Pearl River, and the Heilongjiang water systems in China. Previously, different studies have taken grass carp as the research object [39,40]. Therefore, grass carp, as a typical migratory freshwater fish, was suitable for the central analyzing of the experimental results of this paper. At the same time, to analyze the fish pipeline’s adaptability to different fish, other migratory fish were also mentioned in the discussion.

3. Results and Discussion

3.1. Model Selection Analysis

Figure 6 shows the simulation test results of the fish passage pipeline composed of two Tesla valves under different working conditions. In comparison to Figure 6, when the slope changes in the range of 0~10%, it could be seen that the slope change had little impact on the flow velocity, while the inlet boundary velocity plays a leading role in the flow velocity in the pipe. The test recorded the maximum flow rate in each vital position area (the vital location area was marked as shown in Figure 7). Under the different working conditions marked in Figure 6, the velocity of each vital position of T45-R decreases compared with GMF. The corresponding results are shown in Table 2, recording the velocity control comparison of the average velocity of vital positions in each scenario. When the slope and velocity change within different working conditions set in this section, the relative velocity control ability of T45-R will weaken with the increase in inlet velocity (i.e., with the increase in flow). However, its velocity control performance can still be better than GMF under common working conditions. In addition, under various working conditions, the global maximum speed range of the T45-R Tesla valve was from 0.936 m/s to 2.948 m/s, while the global maximum velocity range of the GMF Tesla valve was 1.157~3.702 m/s. The results illustrated that the global maximum velocity of the T45-R Tesla valve was about 20% lower than that of the GMF Tesla valve. In this paper, the velocity was mainly considered for judging and selecting a model structure, so the T45-R Tesla valve was selected as the final simulation object.

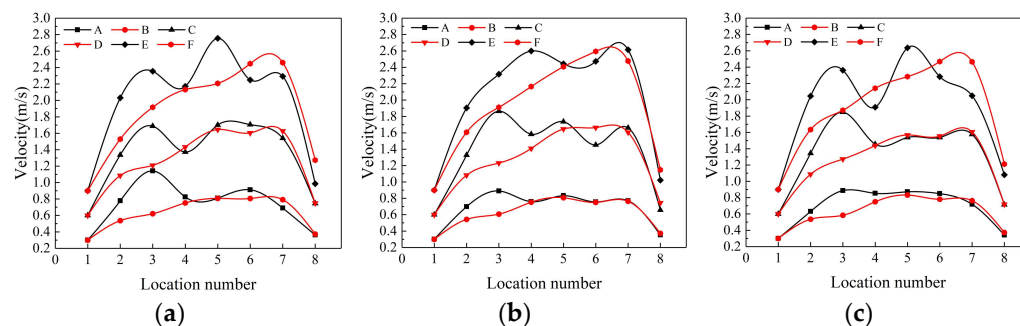


Figure 6. Velocity at vital locations of two Tesla pipelines under different slopes ((a). slope = 0%, (b). slope = 5%, (c). slope = 10%. Black lines A, C, and E are for GMF Tesla valve, and the initial speeds are 0.3 m/s, 0.6 m/s, and 0.9 m/s, respectively; red lines B, D, and F are for T45-R Tesla valve, with initial speeds of 0.3 m/s, 0.6 m/s, and 0.9 m/s, respectively).

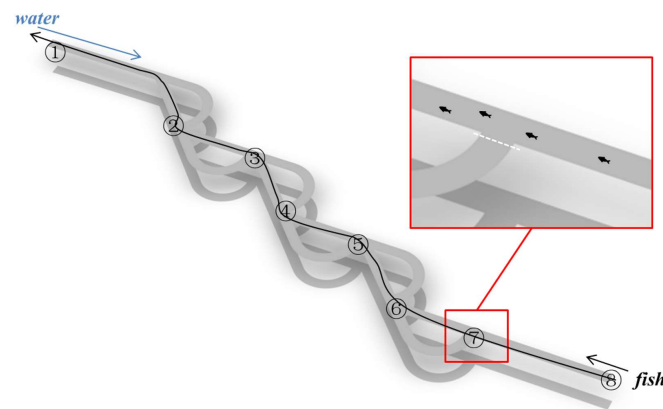


Figure 7. Schematic diagram of fish ascending in the fish passage pipeline (the vital positions for testing have been marked with numbers in the figure).

Table 2. Average percentage of T45-R at each vital position lower than GMF velocity (%).

Working Condition	0%	5%	10%
0.3 m/s	13.74	10.87	11.33
0.6 m/s	7.67	9.56	7.76
0.9 m/s	8.15	8.61	2.28

3.2. Analysis of Turbulence Characteristics

For the T45-R Tesla valve finally selected, further simulation was carried out. Small-sized models were no longer used, but the large-scale model (10:1) was adopted to be more in line with the actual construction (the proportion of the model inlet section was 1000 mm × 1000 mm) [41]. In order to find a reference and control the boundary conditions in the above comparison test conditions, the boundary condition was set to the classical velocity (0.5 m/s), which was converted into the inlet flow, i.e., 0.5 m³/s according to the inlet proportion, and the corresponding setting of 1.5% was also adopted for the slope [42].

As for the analysis of the results, the middle section (500 mm high) was selected as a typical representative for analysis. The velocity cloud diagram is shown in Figure 8. From the velocity distribution, it was easily found that the high-velocity area was mainly concentrated in the circuit of the valve unit. In contrast, the phenomenon close to the still water area appeared on the main road. The black line marked the expected upstream route of grass carp in Figure 7. Fish were not expected to enter the unit circuit, as this was inappropriate (as shown in the local enlarged drawing, the area at the bottom of the white line is not expected to migrate; measures such as fish net could be considered in actual experiments). At this time, the main consideration of migratory grass carp was to pass through the high-velocity area of the main road, and the flow field distribution in this area was close to the jet state. Through the high-velocity area, grass carp can enter the low-velocity area close to still water for rest adjustment. The maximum velocity in the high-velocity area at each vital position was about 0.904 m/s, 1.083 m/s, 1.098 m/s, 1.375 m/s, 1.478 m/s, and 1.284 m/s, respectively (i.e., marked areas 2~7 in Figure 7), and the global average velocity was 0.54 m/s. In Figure 8, consistent with the research of other scholars, with the increase in the number of stages of Tesla valves, the flow rate of corresponding stages along the fluid direction will also have a corresponding increase trend [43,44]. Corresponding to the fishway, this phenomenon was that the speed of the downstream was slightly higher than that of the upstream, and this rule may benefit the fish migration. Because, in terms of the continuous upstream direction of fish, this velocity showed a trend of overall upstream decline, it may be appropriate for the continuous migration of fish.

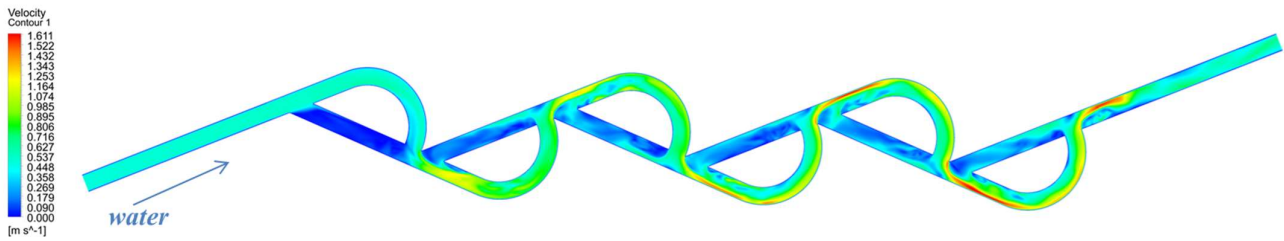


Figure 8. Velocity distribution cloud map.

According to the research [45], the swimming ability parameters of grass carp are shown in Table 3:

Table 3. Swimming ability of grass carp of different sizes.

Grass Carp	Body Length (m)	Burst Swimming Speed (m/s)
Sub-adults fish	0.5124 ± 0.0324	2.899 ± 0.457
Young fish	0.1793 ± 0.0127	2.359 ± 0.434
Juvenile fish	0.0847 ± 0.0073	1.449 ± 0.424

According to the experiment [46], the suitable velocity range of grass carp migration was 0.4~1.0 m/s, and the minimum induced velocity of stimulating grass carp migration was 0.2 m/s. In the simulation, it was found that the average velocity of the middle section of the fish passage pipeline designed based on T45-R was about 0.54 m/s, which was in the range of appropriate velocity. Both the velocity of the upstream and downstream boundaries were higher than the migration-induced velocity. Therefore, the flow velocity in T45-R can stimulate the migration behavior of grass carp. At the same time, the variation range of flow velocity at the vital migration location was 0.904~1.478 m/s, and the high-flow-velocity area was narrow. As shown in Figure 9, sub-adult fish and young fish can easily break through this obstacle and enter the low-flow-velocity area for short-term rest. For juveniles, although their burst migration speed was similar to the maximum velocity at the vital migration location, according to the velocity distribution cloud map, the maximum velocity only existed at a certain point at the marked location. Juveniles can still find a position lower than their burst velocity within the marked location area for breakthrough migration.

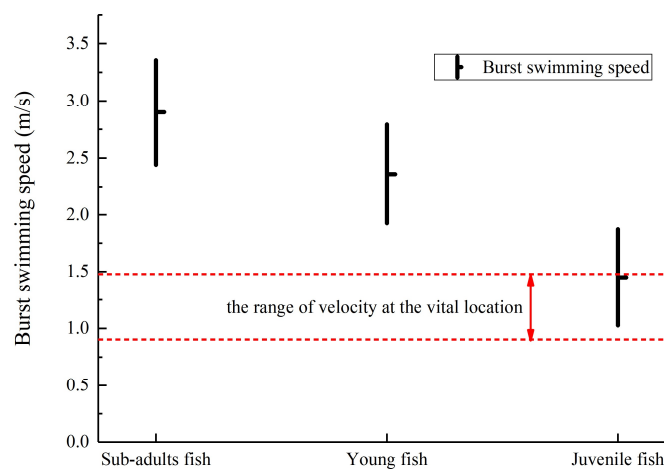


Figure 9. The burst swimming speed of grass carp with different body length.

In order to analyze the applicability of the fish passage pipeline to different fish species, it can be seen that the burst swimming speed of different kinds of fish was basically within the variation range of the maximum velocity at the vital position of the fish passage pipeline

(Table 4 and Figure 10) [47]. The specific comparison result was that the swimming ability of *Mylopharyngodon piceus*, *Aristichthys nobilis*, *Schizothorax macropogon*, and *Ptychobarbus dipogon* under the marked body length specification was just in line with the flow velocity range at the vital position of the fishway under study. The adaptability of *Schizothorax oconnori*, *Racoma waltoni*, and *Oxygymnocypris stewarti* could be better. It can be seen from the analysis in the figure that the fish mentioned above have a high probability of adapting to the velocity field of the fishway under study. Therefore, it can be seen that the fish passage pipeline should have specific adaptability to the migration of some different fishes. However, it was also easy to see that this adaptability had certain limitations. Some fish individuals may not fully adapt to the flow velocity range (such as *Hypophthalmichthys molitrix*, *Schizopygopsis malacanthus*, and *Gymnodiptychus dybowskii*). However, it can show that the fish passage has a certain application potential. In addition, only the swimming ability of some fish was listed here, and the migration adaptability of more fish is worth more discussion in the future. The potential fish passage pipes may require more work to ensure that different fish species can overcome the flow velocity at different vital locations. Therefore, to better adapt to the migration of different kinds of fish, it is necessary to consider optimizing the flow rate control of the fish passage pipeline in the future. For example, it may be optimized from the perspective of its structure.

Table 4. Swimming ability of different fish species.

NO.	Species (Scientific Name)	Body Length (m)	Burst Swimming Speed (m/s)
1	<i>Mylopharyngodon piceus</i>	0.265 ± 0.145	1.22 ± 0.19
2	<i>Hypophthalmichthys molitrix</i>	0.905 ± 0.385	0.96 ± 0.34
3	<i>Aristichthys nobilis</i>	0.185 ± 0.035	1.10 ± 0.12
4	<i>Schizothorax oconnori</i>	0.267 ± 0.036	1.53 ± 0.24
5	<i>Schizothorax macropogon</i>	0.253 ± 0.034	1.22 ± 0.15
6	<i>Racoma waltoni</i>	0.305 ± 0.047	1.37 ± 0.17
7	<i>Oxygymnocypris stewarti</i>	0.216 ± 0.016	1.38 ± 0.20
8	<i>Ptychobarbus dipogon</i>	0.253 ± 0.050	1.10 ± 0.18
9	<i>Schizopygopsis malacanthus</i>	0.109 ± 0.023	0.92 ± 0.08
10	<i>Gymnodiptychus dybowskii</i>	0.182 ± 0.023	1.06 ± 0.18

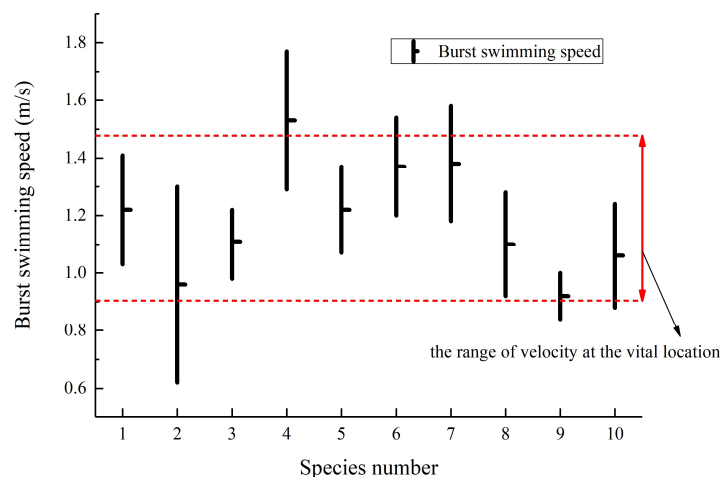


Figure 10. The burst swimming speed of different fish species.

Further, the vector flow field was analyzed. In order to reduce the influence of the inlet and outlet on the flow pattern analysis, two units near the middle were selected for analysis (Figure 11). The valve's low-velocity and high-velocity areas were caused by the hedging effect of water flow, making the eddy phenomenon appear in some low-velocity areas. Specifically, the eddy represents the whirlpool formed by the flow velocity vector in the fishway, which can reflect the collision relationship between the high-velocity area

and the low-velocity area in the fishway. It reflects the active degree of the flow [48]. It can be seen from Figure 11 that the generated multiple eddies mainly appear at the inner side of the jet impingement area of the main migration channel and along the direction of the downstream pointing to the upstream. With the distance from the unit node, the eddies gradually decreased. At the place where the eddy mainly occurs, the maximum size of a single eddy could account for about 50% of the channel width. Combined with the complex flow pattern caused by multiple eddies here, it seems that fish migration could pose a certain challenge. However, some of the water jets and eddies connecting the nodes were just distributed on both sides of the channel, and the direction of the water jet at this position was toward the upstream. If the fish can get close to the flow, the impact of the eddy could be greatly reduced. In addition, according to the statistics, the proportion of eddy-free areas in the low-velocity areas where eddies occur was about 70%, which could indicate that most of the fish in the migration area may not be affected by the eddy [49]. At the same time, the eddy velocity was not high, and the impact on the migration of grass carp could be minimal. Moreover, the eddy formed was mainly horizontal, and the existence of the eddy was conducive to the rest of the fish [50].

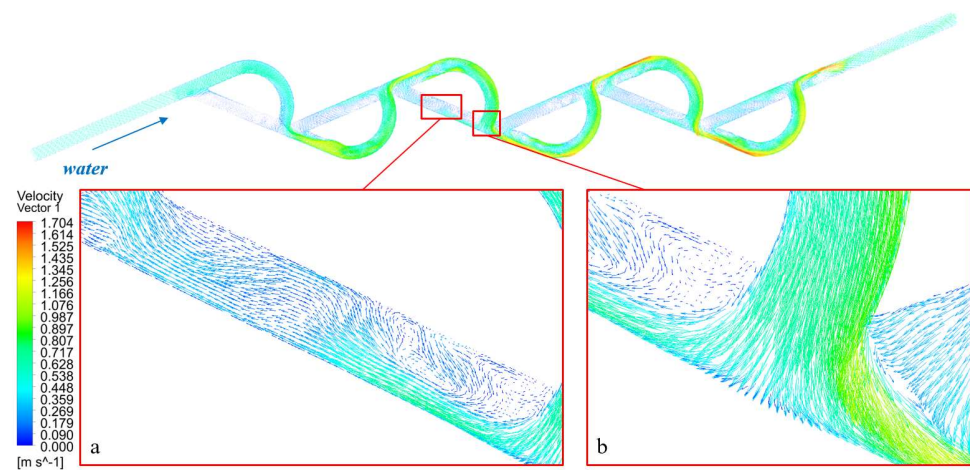


Figure 11. Velocity vector cloud distribution ((a) main migration channel, (b) unit node).

Turbulent kinetic energy (TKE) was one of the critical factors that determined the upstream energy consumption of fish [51]. The typical value of turbulent kinetic energy corresponding to the maximum amplitude under the slope of 1.5% was 0.28–0.80 m²/s², and the turbulent kinetic energy value of the pond chamber fishway was only 0.07 m²/s² [27,52]. According to the obtained turbulence kinetic energy cloud in Figure 12, it can be seen that the fish passage pipeline can better control the turbulence kinetic energy in the global range. From the changing trend of TKE, the TKE in the downstream was higher than in the upstream, which may make it easier for fish to migrate in continuous energy consumption. The same analysis can also be obtained from the velocity analysis mentioned above. At the same time, the TKE value in most areas of the fish passage pipeline was minimal, which was found to be suitable for fish swimming continuously [27]. It was accessible from the figure's distribution of TKE that the more significant value of TKE mainly occurred in the pipeline circuit and jet generation area. The phenomenon may be mainly due to the large flow velocity in the loop area and the significant velocity fluctuation near the vital migration position, so the corresponding TKE value was also high. According to the ideal migration route, the fish in this area passed through a short time or did not pass through, so it was more friendly for fish migration.

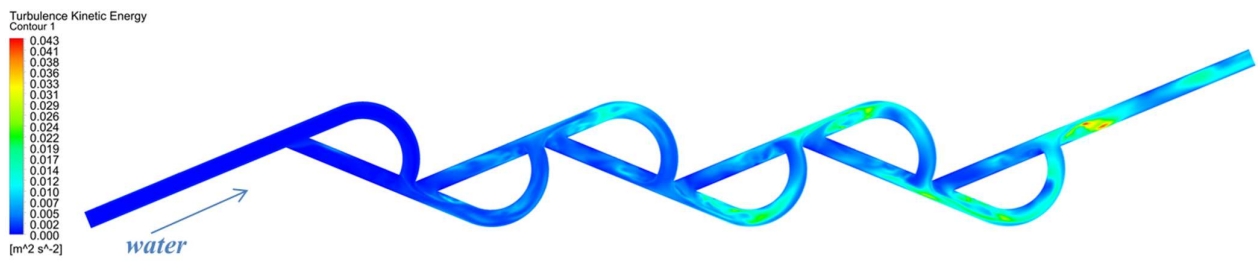


Figure 12. Cloud diagram of turbulent kinetic energy distribution.

Figure 13 shows the distribution characteristics of the turbulent energy dissipation rate inside the channel, and the general rule was similar to TKE. Although the TKE value on the ideal route was high, its turbulent scale was relatively large [53]. Therefore, the corresponding turbulent energy dissipation rate was low, and its maximum value was about $0.089 \text{ m}^2/\text{s}^3$. The turbulent energy dissipation rate in the loop area was generally more prominent than that in the main channel, with a sudden increase. The main reason may be the sudden decrease in turbulent scale [54].

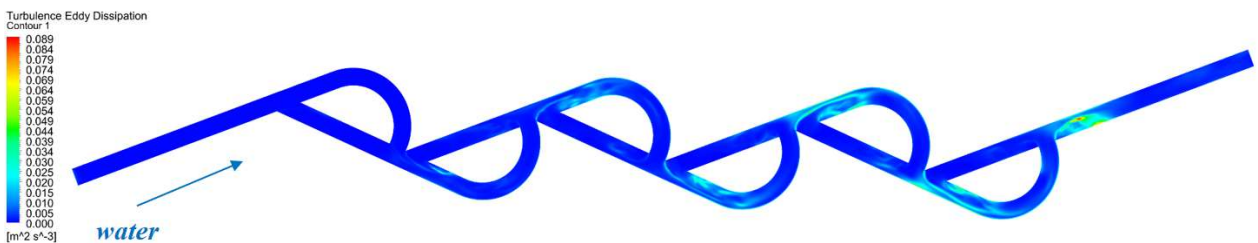


Figure 13. Cloud diagram of turbulent eddy dissipation.

In addition, for closed channels, pressure-related issues were an essential criterion for judging whether they could be used as fish passing facilities. It can be seen from Figure 14 that the pressure distribution was also consistent with the research of many scholars on check valves and the pressure distribution was divided between units [55]. According to the research of Stephenson, et al. [56], the minimum pressure value and pressure gradient in fish passing facilities may cause damage to fish. In this study, the pressure obtained from the postprocessing of the established model was positive in most areas. The calculated pressure gradient that fish need to bear was only $3.321\sim 6.261 \text{ kPa/s}$, according to the pressure gradient in Figure 15. Fish migration is a spontaneous behavior, and the potential risk caused by pressure gradient was expressed here by the product of the fish’s burst swimming speed and pressure gradient. The mean value of grass carp burst speed was 2.236 m/s (Table 3), and the mean value of the remaining 10 samples was 1.186 m/s (Table 4). Higher pressure gradient was only generated between stages, where the pressure change value was significant. Research has shown that the maximum pressure gradient in the process of pressure rise in environmentally friendly hydraulic facilities should be less than 15 kPa/s [57]. Under the working conditions in this paper, the pressure gradient value was far less than the threshold value that may affect fish.

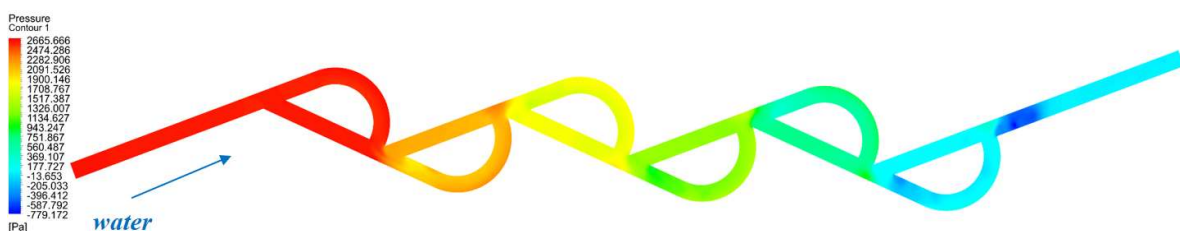


Figure 14. Cloud diagram of pressure distribution.

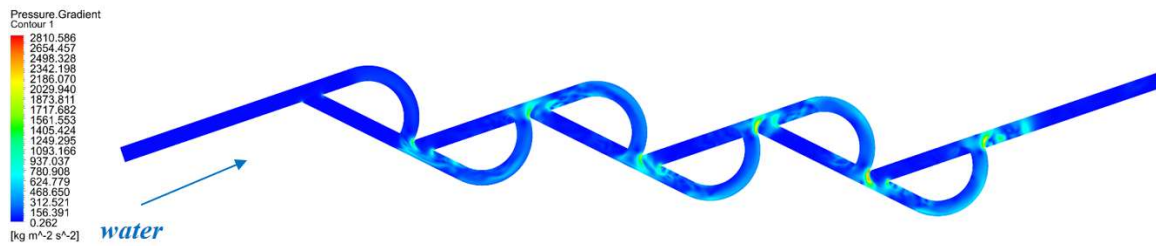


Figure 15. Cloud diagram of pressure gradient.

Nonetheless, it can be seen from Figure 14 that negative pressure occurs in a few downstream areas. This phenomenon may be caused by cavitation, which usually occurs when the fluid in the fluid equipment flows through the throttling element and the flow rate increases [58]. Although the negative pressure area was far less than the positive pressure area, the negative pressure position will probably pass through the downstream fish migration. Therefore, this phenomenon may have a certain impact on fish migration. However, the current judgment was that the impact might be minimal, because the minimum pressure value was only about -0.78 kPa, which was far away from the negative pressure value of damage studied by many scholars (usually reaching the negative level of tens of kilopascals) [54,59]. Therefore, to solve this problem, further consideration should be given to more reasonable optimization of the structure in the future to reduce the impact of this phenomenon. In general, problems related to pressure may have little impact on the fish movement in the fish migration channel. It seems that the research on pressure-related issues needs to be expanded more richly in the future, because it was far from enough only to consider not causing damage to migratory fish. It was also necessary to consider the specific situation of this factor to study the sports metabolism of fish migration and whether there will be stress response and other issues. In particular, the research needed to consider more tests under different working conditions (the current research was only based on the test that can be referred to). This part of the problem may need to be carried out in combination with biological experiments in the later stage.

4. Conclusions

This article was presented to judge whether the Tesla valve can be used as a fish passage pipeline. A fishway pipeline composed of two commonly used Tesla valves was used for preliminary numerical simulation. The model with good speed control was determined by the preliminary simulation test and it was used for further simulation. Then, based on the swimming ability index of grass carp migration, the different parameters of the fish pipeline were analyzed in the results of further numerical simulation. The main conclusions were as follows:

(1) T45-R Tesla valve was better than the GMF Tesla valve in controlling the flow rate at the vital position of migration, and the global maximum speed of the T45-R Tesla valve was about 20% lower than that of the GMF Tesla valve. Therefore, T45-R could be a better choice for the fish passage pipeline.

(2) The average flow velocity was 0.54 m/s, and the flow velocity range at vital positions was 0.904–1.478 m/s, which was consistent with the swimming ability of grass carp. According to the velocity contour, the low-velocity area generated by the reverse flow in the valve can provide a short resting area for grass carp upstream. However, in the analysis of the burst speed rate of different fish, the adaptability of the fish passage pipeline was general, which could not ensure that multiple fish species overcome the flow rate at vital positions. Therefore, further pipeline optimization in flow rate control needs to be considered.

(3) It can be seen from the velocity vector cloud map of the fish passing pipeline that certain vortices will be generated in the low-velocity area of the main pipeline. However,

according to the analysis, the low-speed horizontal vortices have little impact on fish migration.

(4) The maximum turbulent kinetic energy of the fish passage pipeline in this design is $0.043 \text{ m}^2/\text{s}^2$, and the high value of turbulent kinetic energy generally appeared in the valve circuit. However, in most ideal migration areas, the turbulent kinetic energy was low, which was suitable for fish upstream.

(5) From the analysis of pressure distribution results, the channel was basically in a positive pressure state, so the risk of fish damage may be low. However, a small number of negative pressure areas needed to be paid attention to. This part of the research needed to be combined with structural adjustment and discussion, which may be to optimize the parameters of the original structure or to design the original structure as open. The maximum value of the pressure gradient of the object was only about 6.261 kPa, which could not reach the threshold value of damage to fish. However, this was only limited to the working conditions in this paper, and whether it had a specific impact on the movement of fish during migration needs to be discussed more in the future.

From the perspective of turbulent characteristic parameters, the Tesla valve has the potential to be applied to the fish passage pipeline. However, only considering the turbulence characteristics has limitations. Only the prospect of Tesla valve application in the fish passage has been explored. In future work, related research could consider the application possibility of fish pipelines from more perspectives, hydraulic model experiment, and biological test. In addition, not only the form of a pipeline but also the model test of reconstruction may be involved in future work. The possible reconstruction direction of this part is to design it as an open fishway in combination with the conventional fishway of the tank room. The working environment setting may also be combined with the fish release for more comprehensive design tests.

Author Contributions: Conceptualization, G.Z.; Funding acquisition, M.X.; Investigation, G.Z.; Methodology, M.X.; Project administration, J.M.; Supervision, J.M.; Validation, C.H.; Visualization, C.F.; Writing—original draft, G.Z. and M.X.; Writing—review and editing, G.Z. and M.X. All authors have read and agreed to the published version of the manuscript.

Funding: This work was financially supported by the National Natural Science Foundation of China (Project No. 51909235), Zhejiang Province Public Welfare Technology Application Research Project (Project No. LGG22E090001), Zhejiang Post-Doctoral Preferential Fund Project (Project No. ZJ2021115), and Zhejiang Provincial Education Department Special Project for Professional Degree Postgraduates (Project No. Y202249406).

Institutional Review Board Statement: Not applicable.

Informed Consent Statement: Not applicable.

Data Availability Statement: Not applicable.

Conflicts of Interest: The authors declare no conflict of interest.

References

1. Singh, V.K.; Nath, T. Energy generation by small hydro power plant under different operating condition. *Int. J. Hydromechatronics* **2021**, *4*, 331–349. [[CrossRef](#)]
2. Romão, F.; Quaresma, A.L.; Santos, J.M.; Amaral, S.D.; Branco, P.; Pinheiro, A.N. Multislot fishway improves entrance performance and fish transit time over vertical slots. *Water* **2021**, *13*, 275. [[CrossRef](#)]
3. Baharvand, S.; Lashkar-Ara, B. Hydraulic design criteria of the modified meander C-type fishway using the combined experimental and CFD models. *Ecol. Eng.* **2021**, *164*, 106207. [[CrossRef](#)]
4. Lucas, M.; Baras, E. *Migration of Freshwater Fishes*; John Wiley & Sons: Hoboken, NJ, USA, 2008.
5. Sanz-Ronda, F.J.; Fuentes-Pérez, J.F.; García-Vega, A.; Bravo-Córdoba, F.J. Fishways as downstream routes in small hydropower plants: Experiences with a potamodromous cyprinid. *Water* **2021**, *13*, 1041. [[CrossRef](#)]
6. Pavlova, A.; Beheregaray, L.B.; Coleman, R.; Gilligan, D.; Harrisson, K.A.; Ingram, B.A.; Kearns, J.; Lamb, A.M.; Lintermans, M.; Lyon, J. Severe consequences of habitat fragmentation on genetic diversity of an endangered Australian freshwater fish: A call for assisted gene flow. *Evol. Appl.* **2017**, *10*, 531–550. [[CrossRef](#)] [[PubMed](#)]

7. Cao, Q.; Yang, W.; Zhuo, L. Review on Study of Fishery Facilities at Home and Abroad. *J. Yangtze River Sci. Res. Inst.* **2010**, *27*, 39–43. [[CrossRef](#)]
8. Birnie-Gauvin, K.; Franklin, P.; Wilkes, M.; Aarestrup, K. Moving beyond fitting fish into equations: Progressing the fish passage debate in the Anthropocene. *Aquat. Conserv. Mar. Freshw. Ecosyst.* **2019**, *29*, 1095–1105. [[CrossRef](#)]
9. Sanagiotto, D.G.; Rossi, J.B.; Bravo, J.M. Applications of Computational Fluid Dynamics in The Design and Rehabilitation of Nonstandard Vertical Slot Fishways. *Water* **2019**, *11*, 199. [[CrossRef](#)]
10. Mao, X. Review of fishway research in China. *Ecol. Eng.* **2018**, *115*, 91–95. [[CrossRef](#)]
11. Katopodis, C.; Williams, J.G. The development of fish passage research in a historical context. *Ecol. Eng.* **2012**, *48*, 8–18. [[CrossRef](#)]
12. Jaziri, N.; Boughamoura, A.; Müller, J.; Mezghani, B.; Tounsi, F.; Ismail, M. A comprehensive review of Thermoelectric Generators: Technologies and common applications. *Energy Rep.* **2020**, *6*, 264–287. [[CrossRef](#)]
13. Keizer, K. Determination Whether a Large Scale Tesla Valve Could Be Applicable as a Fish Passage. Additional Thesis, Delft University of Technology, Delft, The Netherlands, October 2016.
14. Kroes, M.; Monden, S. *Vismigratie. Een Handboek Voor Herstel in Vlaanderen en; Aminal, Afdeling Water: Brussel, Belgium, 2005.*
15. Jin, Z.; Gao, Z.; Chen, M.; Qian, J. Parametric study on Tesla valve with reverse flow for hydrogen decompression. *Int. J. Hydrogen Energy* **2018**, *43*, 8888–8896. [[CrossRef](#)]
16. Porwal, P.R.; Thompson, S.M.; Walters, D.K.; Jamal, T. Heat transfer and fluid flow characteristics in multistaged Tesla valves. *Numer. Heat Transf. Part A Appl.* **2018**, *73*, 347–365. [[CrossRef](#)]
17. He, C.; Gu, Y.; Zhang, J.; Ma, L.; Yan, M.; Mou, J.; Ren, Y. Preparation and modification technology analysis of ionic polymer-metal composites (IPMCs). *Int. J. Mol. Sci.* **2022**, *23*, 3522. [[CrossRef](#)] [[PubMed](#)]
18. Tarrade, L.; Pineau, G.; Calluaud, D.; Texier, A.; David, L.; Larinier, M. Detailed experimental study of hydrodynamic turbulent flows generated in vertical slot fishways. *Environ. Fluid Mech.* **2011**, *11*, 1–21. [[CrossRef](#)]
19. Dong, Z.; Yu, J.; Huang, Z. Experimental Study on Turbulence Structure of Combined Fishway with Overflow Weir and Vertical Joint. *Advances in Water Science* **2021**, *32*, 279–285. [[CrossRef](#)]
20. Duarte, B.A.D.F.; Ramos, I.C.R.; Santos, H.D.A. Reynolds shear-stress and velocity: Positive biological response of neotropical fishes to hydraulic parameters in a vertical slot fishway. *Neotrop. Ichthyol.* **2012**, *10*, 813–819. [[CrossRef](#)]
21. Cea, L.; Pena, L.; Puertas, J.; Vázquez-Cendón, M.; Peña, E. Application of several depth-averaged turbulence models to simulate flow in vertical slot fishways. *J. Hydraul. Eng.* **2007**, *133*, 160–172. [[CrossRef](#)]
22. Luo, H.; Zhou, P.; Shu, L.; Mou, J.; Zheng, H.; Jiang, C.; Wang, Y. Energy Performance Curves Prediction of Centrifugal Pumps Based on Constrained PSO-SVR Model. *Energies* **2022**, *15*, 3309. [[CrossRef](#)]
23. Heimerl, S.; Hagemeyer, M.; Echterler, C. Numerical flow simulation of pool-type fishways: New ways with well-known tools. *Hydrobiologia* **2008**, *609*, 189–196. [[CrossRef](#)]
24. Fuentes-Perez, J.F.; Silva, A.T.; Tuhtan, J.A.; Garcia-Vega, A.; Carbonell-Baeza, R.; Musall, M.; Kruusmaa, M. 3D modelling of non-uniform and turbulent flow in vertical slot fishways. *Environ. Model. Softw.* **2018**, *99*, 156–169. [[CrossRef](#)]
25. Marriner, B.A.; Baki, A.B.M.; Zhu, D.Z.; Cooke, S.J.; Katopodis, C. The hydraulics of a vertical slot fishway: A case study on the multi-species Vianney-Legendre fishway in Quebec, Canada. *Ecol. Eng. J. Ecotechnol.* **2016**, *90*, 190–202. [[CrossRef](#)]
26. Barton, A.F.; Keller, R.J. 3D Free Surface Model of a Vertical Slot Fishway. In Proceedings of the IAHR Congress, Bergen, Norway, 8–10 May 2003.
27. Silva, A.T.; Santos, J.M.; Ferreira, M.T.; Pinheiro, A.N.; Katopodis, C. Effects of Water Velocity and Turbulence on the Behaviour of Iberian Barbel (*Luciobarbus bocagei*, Steindachner 1864) in an Experimental Pool-Type Fishway. *River Res. Appl.* **2011**, *27*, 360–373. [[CrossRef](#)]
28. Martins, K.L.; Silva, R.B.D.; Silvestre, G.M.; Pinto, V.T.; Santos, E.D.d.; Isoldi, L.A.; Rocha, L.A.O. Constructural design applied to geometrical analysis of a triangular arrangement of H-Darrieus wind turbines. *Int. J. Hydromechatronics* **2020**, *3*, 155–166. [[CrossRef](#)]
29. Kumar, S.; Verma, K.A.; Pandey, K.M.; Sharma, K.K. A review on methods used to reduce drag of the ship hulls to improve hydrodynamic characteristics. *Int. J. Hydromechatronics* **2020**, *3*, 297–312. [[CrossRef](#)]
30. Qian, J.; Chen, M.; Liu, X.; Jin, Z. A numerical investigation of the flow of nanofluids through a micro Tesla valve. *J. Zhejiang Univ. Sci. A* **2018**, *20*, 50–60. [[CrossRef](#)]
31. Gamboa, A.R.; Morris, C.J.; Forster, F.K. Improvements in Fixed-Valve Micropump Performance Through Shape Optimization of Valves. *J. Fluids Eng.* **2005**, *127*, 339–346. [[CrossRef](#)]
32. Yuan, X.; He, Z.; Mao, G. Numerical Simulation of a Turbulence Flow in the Cut-off Valve by RNG k- ϵ Turbulence Model. *Fluid Mach.* **2006**, *34*, 5. [[CrossRef](#)]
33. Wei, Y.; Luo, K.; Tan, J.; Tang, L.; Wang, J. Study on Hydraulic Characteristics of Vertical Slot Fishway Based on Three Turbulence Models. *Water Resour. Power* **2020**, *38*, 71–74+78.
34. Bao, Y.; Wang, H. Numerical study on flow and heat transfer characteristics of a novel Tesla valve with improved evaluation method. *Int. J. Heat Mass Transf.* **2022**, *187*, 122540. [[CrossRef](#)]
35. Xu, M.; Zeng, G.; Wu, D.; Mou, J.; Zhao, J.; Zheng, S.; Huang, B.; Ren, Y. Structural Optimization of Jet Fish Pump Design Based on a Multi-Objective Genetic Algorithm. *Energies* **2022**, *15*, 4104. [[CrossRef](#)]
36. Gu, Y.; Zhang, J.; Yu, S.; Mou, C.; Li, Z.; He, C.; Wu, D.; Mou, J.; Ren, Y. Unsteady numerical simulation method of hydrofoil surface cavitation. *Int. J. Mech. Sci.* **2022**, *228*, 107490. [[CrossRef](#)]

37. Sullivan, C.J.; Weber, M.J.; Pierce, C.L.; Camacho, C.A. A Comparison of Grass Carp Population Characteristics Upstream and Downstream of Lock and Dam 19 of the Upper Mississippi River. *J. Fish Wildl. Manag.* **2020**, *11*, 99–111. [[CrossRef](#)]
38. Masser, M.P. *Using Grass Carp in Aquaculture and Private Impoundments*; SRAC: Mississippi, MS, USA, 2002.
39. Mu, X.; Zhen, W.; Li, X.; Cao, P.; Gong, L.; Xu, F. A Study of the Impact of Different Flow Velocities and Light Colors at the Entrance of a Fish Collection System on the Upstream Swimming Behavior of Juvenile Grass Carp. *Water* **2019**, *11*, 322. [[CrossRef](#)]
40. Xu, M.; Ji, B.; Zou, J.; Long, X. Experimental investigation on the transport of different fish species in a jet fish pump. *Aquac. Eng.* **2017**, *79*, 42–48. [[CrossRef](#)]
41. Wen, Y.; Chen, R.-F. Study on seepage characteristics of large scale Tesla valve and feasibility of its application in water pipeline. *J. Hydrodyn.* **2020**, *35*, 10. [[CrossRef](#)]
42. Novak, G.; Domínguez, J.M.; Tafuni, A.; Silva, A.T.; Pengal, P.; Četina, M.; Žagar, D. 3-D Numerical Study of a Bottom Ramp Fish Passage Using Smoothed Particle Hydrodynamics. *Water* **2021**, *13*, 1595. [[CrossRef](#)]
43. Qian, J.; Chen, M.; Gao, Z.; Jin, Z. Mach number and energy loss analysis inside multi-stage Tesla valves for hydrogen decompression. *Energy* **2019**, *179*, 647–654. [[CrossRef](#)]
44. Mohammadzadeh, K.; Kolahdouz, E.; Shirani, E.; Shafii, M. Numerical Investigation on the effect of the size and number of stages on the Tesla microvalve efficiency. *J. Mech.* **2013**, *29*, 527–534. [[CrossRef](#)]
45. Lu, B.; Liu, W.; Liang, Y.; Chen, Q.; Huang, Y.; Pan, L.; Liu, D.; Shi, X. The burst-coast swimming behavior of grass carp (*Ctenopharyngodon idellus*) during fast-start. *J. Fish. China* **2014**, *38*, 6. [[CrossRef](#)]
46. Yang, Q.; Hu, P.; Yang, Z.; Chu, L.; Yang, J. Suitable Flow Rate and Adaptive Threshold for Grass Carp (*Ctenopharyngodon idellus*) Migration. *J. Hydroecology* **2019**, *40*, 8. [[CrossRef](#)]
47. General Institute of Water Resources and Hydropower Planning and Design. *Guidelines for Fishway Design of Water Conservancy and Hydropower Projects*; SL 609-2013; China Water & Power Press: Beijing, China, 2013.
48. Yan, B.; Kells, J.A.; Sparling, B.F.; Garner, M.E.; Katopodis, C. Turbulence Characteristics of the Flow in a Corrugated Steel Pipe Culvert in the Context of Fish Passage. In Proceedings of the 20th Canadian Hydrotechnical Conference, Ottawa, ON, Canada, 14–17 June 2011.
49. Gao, F. Study on seepage characteristics of water conservancy facilities in fishway in river regulation project. *Hydro Sci. Cold Zone Eng.* **2021**, *6*, 26–31. [[CrossRef](#)]
50. Dong, Z.; Jiang, L.; Mao, B.; Chen, X. An Experimental Study of Turbulent Flow Structures in a Vertical Slot Fishway with Staggered Slots. *J. Hydroecology* **2021**, *42*, 129–136. [[CrossRef](#)]
51. Bravo-Córdoba, F.; Fuentes-Pérez, J.; Valbuena-Castro, J.; Azagra-Paredes, A.; Sanz-Ronda, F. Turning Pools in Stepped Fishways: Biological Assessment via Fish Response and CFD Models. *Water* **2021**, *13*, 1186. [[CrossRef](#)]
52. Baki, A.B.M.; Zhu, D.Z.; Rajaratnam, N. Turbulence Characteristics in a Rock-Ramp-Type Fish Pass. *J. Hydraul. Eng.* **2015**, *141*, 156–168. [[CrossRef](#)]
53. Waterhouse, A.F.; MacKinnon, J.A.; Nash, J.D.; Alford, M.H.; Kunze, E.; Simmons, H.L.; Polzin, K.L.; Laurent, L.C.S.; Sun, O.M.; Pinkel, R.; et al. Global Patterns of Diapycnal Mixing from Measurements of the Turbulent Dissipation Rate. *J. Phys. Oceanogr.* **2014**, *44*, 1854–1872. [[CrossRef](#)]
54. Jiang, Y.; Yang, Z.; Shi, X.; Wu, L.; Nie, L.; Wei, Y. The simulation of fish migratory trajectory in a vertical slot fishway based on multi-hydraulic indices. *Chin. J. Ecol.* **2018**, *37*, 1282–1290. [[CrossRef](#)]
55. Andriukaitis, D.; Vargalis, R.; Šerpytis, L.; Drevinskas, T.; Kornysšova, O.; Stankevičius, M.; Bimbraitė-Survilienė, K.; Kaškonienė, V.; Maruškas, A.S.; Jonušauskas, L. Fabrication of Microfluidic Tesla Valve Employing Femtosecond Bursts. *Micromachines* **2022**, *13*, 1180. [[CrossRef](#)]
56. Stephenson, J.R.; Gingerich, A.J.; Brown, R.S.; Pflugrath, B.D.; Deng, Z.; Carlson, T.J.; Langeslay, M.J.; Ahmann, M.L.; Johnson, R.L.; Seaburg, A.G. Assessing barotrauma in neutrally and negatively buoyant juvenile salmonids exposed to simulated hydro-turbine passage using a mobile aquatic barotrauma laboratory. *Fish. Res.* **2010**, *106*, 271–278. [[CrossRef](#)]
57. Shao, Q.; Li, H.; Wu, Y.; Chen, J. Simulating Experiment on Fish Damage Caused by The Pressure Gradient in Hydraulic Machinery. *J. Mech. Eng.* **2002**, *38*, 7–11. [[CrossRef](#)]
58. Huang, L.; Wang, J.; Hou, L.; Yang, Y. Experimental study on cavitation evolution law and cavitation damage of stop valve. *Fluid Mach.* **2022**, *50*, 1–7. [[CrossRef](#)]
59. Wang, Y.; Zhai, Z.; Yang, L.; Shi, X. Effect of Sudden Pressure Change in Turbine Passages on Juveniles of the Four Major Chinese Carps. *J. Hydroecol.* **2021**, *42*, 86–93. [[CrossRef](#)]

Disclaimer/Publisher’s Note: The statements, opinions and data contained in all publications are solely those of the individual author(s) and contributor(s) and not of MDPI and/or the editor(s). MDPI and/or the editor(s) disclaim responsibility for any injury to people or property resulting from any ideas, methods, instructions or products referred to in the content.